JOURNAL OF CATALYSIS 123, 417–435 (1990)

Oxidative Dehydrogenation of Propane over V–Mg–O Catalysts

D. SIEW HEW SAM,[1] V. SOENEN, AND J. C. VOLTA[2]

Institut de Recherches sur la Catalyse, CNRS, 2, Avenue A. Einstein, 69626 Villeurbanne Cedex, France

Received July 18, 1989; revised October 23, 1989

Oxidative dehydrogenation of propane was studied at 500–550°C over V–Mg–oxide catalysts and over the reference phases orthovanadate, pyrovanadate, and metavanadate of magnesium. Characterization of the reference phases was performed by XRD, IR spectroscopy, TEM, STEM, and ^{51}V NMR and compared with the V–Mg–O catalysts. In contrast with previous results by Kung, it was observed that the actual catalyst for dehydrogenation of propane to propene is pyrovanadate of magnesium. This specificity is explained on the basis of a dynamic model of the working catalyst favored by the corner-sharing VO_4 tetrahedra of the $V_2O_7^{4-}$ units.

INTRODUCTION

The catalytic oxidative dehydrogenation of alkanes to alkenes, dienes, or aromatics is a challenging problem and a fascinating route to convert them into chemicals. However, this catalysis requires high temperatures to activate alkanes, conditions which favor the complete oxidation of the dehydrogenated intermediates.

In order to overcome this problem, it is necessary to find a catalyst which can activate the C–H bond of the alkane and which can provide suitable oxygen atoms, not too reactive for total oxidation. This should depend on the temperature of the reaction, the alkane/oxygen ratio, and the residence time on the catalyst surface.

The V–Mg–O system has been proposed to be efficient for the oxidative dehydrogenation of butane (*1, 2*) and propane (*3*). It was postulated that both reactions proceed via the formation of an alkyl radical.

The same authors proposed that the active phase is magnesium orthovanadate and they suggested that the higher selectivity of this phase was due to the low density of V=O groups responsible for total oxidation.

We have studied the oxidative dehydrogenation of propane to propene on V–Mg–O catalysts with a vanadium content up to 82% (calculated as V_2O_5) in order to cover the composition range of the different magnesium vanadates, and we compared these results with those obtained on reference phases, whose purity was strictly controlled.

In this paper, we report our results of the characterization of the V–Mg–O catalysts, the identification of the active component, and the correlation with the catalytic results.

EXPERIMENTAL

Catalysts and reference phases were prepared from magnesium hydroxide and ammonium vanadate (NH_4VO_3, Merck).

$Mg(OH)_2$ was prepared by precipitation from a magnesium chloride solution ($MgCl_2 \cdot 6H_2O$, Merck, 0.25 *M*) by potassium hydroxide (Prolabo, 0.5 *M*) After a first washing with distilled water, the precipitate was centrifuged and then dried under vacuum at 80°C. The solid thus obtained was freed from any residual chloride ions by washing repeatedly with water until the filtrate had a constant electrical conductivity. The solid was then dried under vacuum at 100°C and immediately used for the preparation of the mixed oxide catalysts in

[1] Present address: ORKEM Co., Norsolor, CRNC, 62670 Mazingarbe.

[2] To whom correspondence should be addressed.

0021-9517/90 $3.00

order to avoid any further carbonation. An appropriate amount of $Mg(OH)_2$ powder was added to a basic aqueous solution (1% NH_4OH) containing NH_4VO_3. The suspension was evaporated to dryness while being stirred and then finally dried at 110°C. The resulting solid was ground into a fine powder and calcined at high temperature for different times. Trace amounts of potassium were detected on the resulting catalysts but K content was always less than 0.02%. The BET areas were determined by nitrogen adsorption in an automatic apparatus constructed at the Institute of Catalysis. Chemical analysis of the elements was carried out by atomic absorption spectrometry.

The catalytic test was performed in a flow system. The catalyst was deposited on a fixed bed in a quartz microreactor (U tube, 13 mm diameter) operating under atmospheric pressure. The catalytic zone was isothermal (6 mm height, 0.8 cm^3 volume) with a precatalytic (1.7 cm^3) and a postcatalytic (0.4 cm^3) zone. Analysis of reactants and reaction products was done by on-line gas chromatography. For the permanent gases and H_2O, a Delsi IGC 120 MB gas chromatograph equipped with a thermal conductivity detector was used. Hydrogen was the carrier gas. Two columns were operated in parallel, a 3-m $\frac{1}{4}$-in. molecular sieve 5A column to separate O_2 and CO and a 2-m $\frac{1}{4}$-in. Porapak Q column to separate CO_2 and H_2O. For the organic products a Delsi IGC 120 FB gas chromatograph equipped with a flame ionization detector was used. Nitrogen was the carrier gas. Three columns were operated in parallel: a 4-m $\frac{1}{8}$-in. Durapak column to separate light hydrocarbons (methane, ethane, ethene, propane, propene), a 3-m $\frac{1}{8}$-in. Carbowax column to separate oxygenates (ethanal, propanal, acetone, acrylaldehyde) and a 2-m $\frac{1}{8}$-in. AT 1200 column to separate acids (acetic, propionic and acrylic acids). This last column was situated in a "hot box" together with the four different injection valves which were monitored by a Spectra Physics computer. The reactor was directly connected to the hot box to prevent any condensation of the reaction products. Catalytic runs were automatically monitored by the computer.

Under the standard condition, the feed was 2 vol% propane (N 99.99, Air Liquide), 19.6% O_2, and 78.4% N_2. The flow rate was 50 ml/min and the reaction temperature was 400 to 550°C. The empty reactor showed no activity (0.63% propane conversion at 550°C). A typical run lasted for about 16 h with four steps at 400, 500, 550, and then 500°C for 2 h. Two analyses were performed at each temperature. No deactivation of the catalyst was observed.

X-ray diffraction was performed using Cu$K\alpha$ radiation on a Siemens goniometer equipped with a quartz front monochromator.

Infrared spectra were obtained between 300 and 1100 cm^{-1} with a Perkin–Elmer 180 spectrophotometer. The catalyst was mixed with KBr (2/300 mg) and pressed into a thin wafer.

For XPS experiments, samples were introduced into a Hewlett–Packard HP 5950 A spectrometer and outgassed at room temperature to a pressure of 10^{-9} Torr. The spectrometer was monitored by a computer and the different spectra were accumulated from 5 min up to 2 h depending on their intensity. The experimental spectra were treated by computer for smoothing, subtraction of the background, and determination of the peak areas.

Electron microscopy investigation was undertaken using a JEOL 100C electron microscope for transmission and diffraction examinations (resolution: 0.3 nm). Microanalysis of the elemental composition of the solids (EDX) was carried out using a STEM (scanning transmission electron microscope) HB5 from Vacuum Generator.

^{51}V NMR spectra were recorded on a BRUKER MSL-300 spectrometer at 75 Hz in the frequency range 125 Khz with a radio frequency duration of 2 μs and a pulse repetition rate of 10 Hz. The used scan accumulation number was from 5×10^3 to 30×10^3.

The chemical shift in the ^{51}V NMR spectra was measured relative to the $VOCl_3$ signal. We used the sample magic-angle spinning method (MAS) at frequency 2.5 kHz in zirconia rotors. Spectra were recorded with and without spinning on the reference phases.

DTA measurements were performed on a MDTA 85 SETARAM over the temperature range 20–1000°C. These studies were carried out on impregnated NH_4VO_3/$Mg(OH)_2$ corresponding to different vanadium contents. The reference material was Al_2O_3 previously ignited at 1100°C. Sample and reference were contained in platinum crucibles set in a ceramic block and the heating rate was 10°C/min. All curves were obtained under a flow of air.

RESULTS

Catalyst Characterization

V–Mg–O catalysts were obtained from impregnated $NH_4VO_3/Mg(OH)_2$ after calcination at 550°C for 6 h. Table 1 lists the compositions and the surface areas of the catalysts. Chemical analysis of V_2O_5 is in good agreement with the nominal V_2O_5 content. A slight discrepancy is observed for the MgO weight content due to the possible presence of $MgCO_3$. The color of the catalysts varied from white for MgO to slightly yellow for catalysts with high vanadium content.

TABLE 1

Characteristics of the VMgO Catalysts

Catalysts	Surface area (m^2/g)	Composition	
		V_2O_5 (wt %)	MgO[a] (wt %)
V_2O_5	2.1	100	0
MgO	142.2	0	100
5 V–Mg–O	130.6	5.0	85.8
13 V–Mg–O	117.6	12.8	80.7
29 V–Mg–O	68.3	29.1	63.2
40 V–Mg–O	42.7	38.0	53.5
48 V–Mg–O	35.2	47.8	47.0
60 V–Mg–O	18.7	58.5	38.0
69 V–Mg–O	11.2	66.4	—
82 V–Mg–O	6.0	79.8	—

[a] Chemical analysis of the elements was done by atomic absorption spectrometry. The MgO content was calculated from the values of Mg on the hypothesis of the unique presence of MgO.

TABLE 2

Characteristics of the Reference Phases

Samples	Surface area (m^2/g)	Composition			
		% V		% Mg	
		Theor.	Exp.	Theor.	Exp.
$Mg_3V_2O_8$	0.9	34.0	34.1	24.0	22.5
$\alpha Mg_2V_2O_7$	1.7	38.9	39.3	18.3	17.1
βMgV_2O_6	0.1	46.0	45.9	11.0	10.3

Magnesium vanadates were prepared from the solids with the corresponding nominal vanadium content. Mg orthovanadate ($Mg_3V_2O_8$) was prepared from the 60 V–Mg–O catalyst calcined in air 6 h at 550°C, 49 h at 625°C, 60 h at 640°C, 15 h at 750°C, and 15 h at 800°C. It was ground between each heating.

α-Mg pyrovanadate ($Mg_2V_2O_7$) was prepared from the 69 V–Mg–O catalyst calcined in air, 6 h at 550°C, 6 h at 600°C, 6 h at 650°C, and 17 h at 700°C. It was ground between each heating. β-Mg metavanadate (MgV_2O_6) was prepared from the 82 V–Mg–O catalyst in air 6 h at 550°C, 6 h at 600°C, and 24 h at 700°C. It was ground between each heating. Table 2 lists the chemical composition and the surface areas of the reference phases. There is a good agreement between the experimental and the theoretical composition.

Results of X-ray diffraction are shown in Fig. 1 for the reference phases. The spectrum for $Mg_3V_2O_8$ (Fig. 1a) is in good agreement with that observed by Lubin (*4*). The purity has been estimated to be 95% with a slight impurity of $\beta Mg_2V_2O_7$ (2θ = 18.9, 28.2) (*5*, *6*). The spectrum for $\alpha Mg_2V_2O_7$ (Fig. 1b) is in good agreement with that observed by Clark (*6*). The purity has been

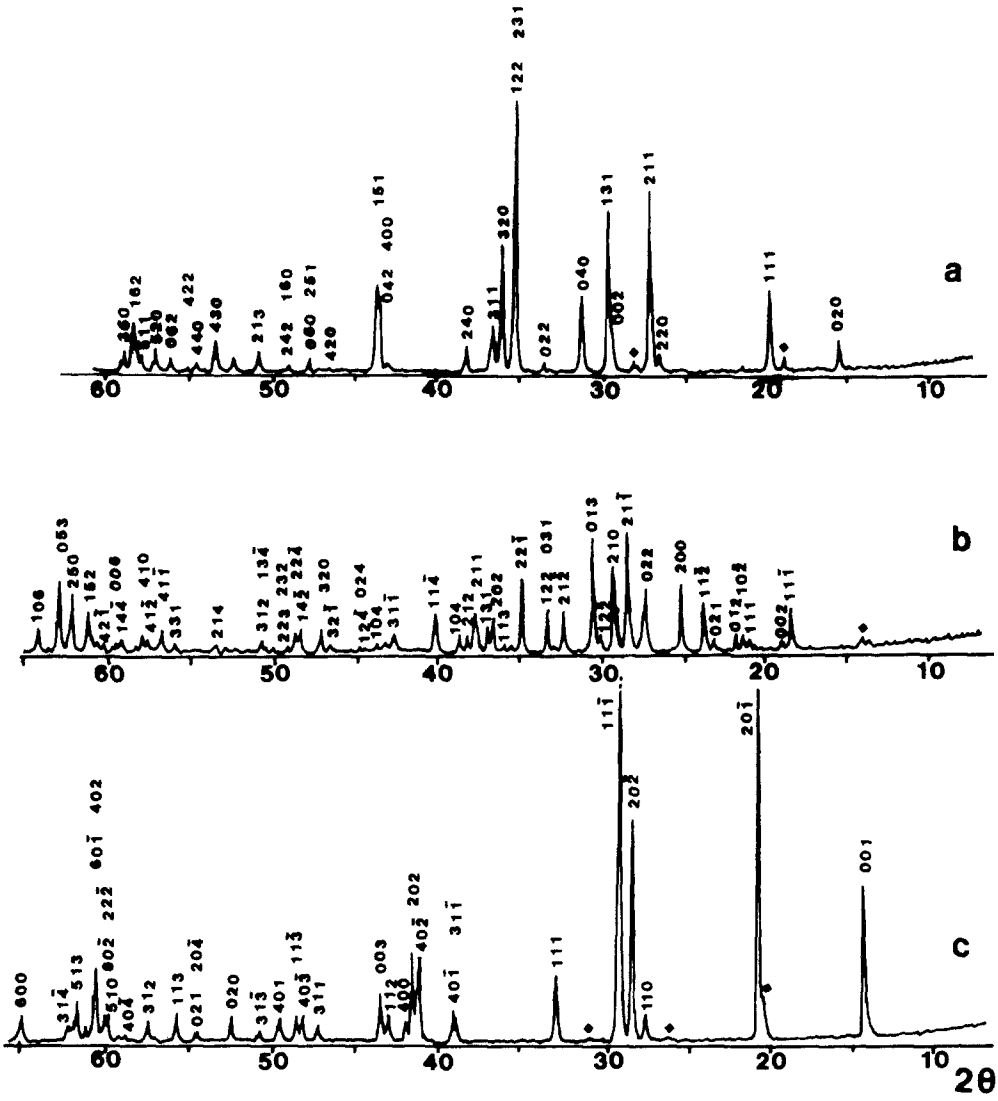

FIG. 1. X-ray diagrams of references phases. (a) $Mg_3V_2O_8$, (◆) impurity $\beta Mg_2V_2O_7$; (b) $\alpha Mg_2V_2O_7$, (◆) impurity βMgV_2O_6; (c) βMgV_2O_6, (◆) impurity αMgV_2O_6.

estimated to be 95% with slight impurity of βMgV_2O_6 ($2\theta = 14.2$) which appeared to be formed at lower calcination temperatures (600°C) but almost disappeared at 700°C. This observation was confirmed by the DTA study. The spectrum for βMgV_2O_6 (Fig. 1c) is in good agreement with the pattern found by Galy and Pouchard (*7*) and Parker and Cauley (*8*). The purity has been estimated to be 98% with a slight impurity of the low-temperature form of αMgV_2O_6 ($2\theta = 20.69, 26.25, 31.06$) (*6*).

The DTA curves obtained for different vanadium contents are presented in Fig. 2. They give interesting data on the temperature of formation of the different vanadates and their further transformations. Taking into account the solid state chemistry study by Clark (*6*), it was possible to assign the different thermal peaks to specific events

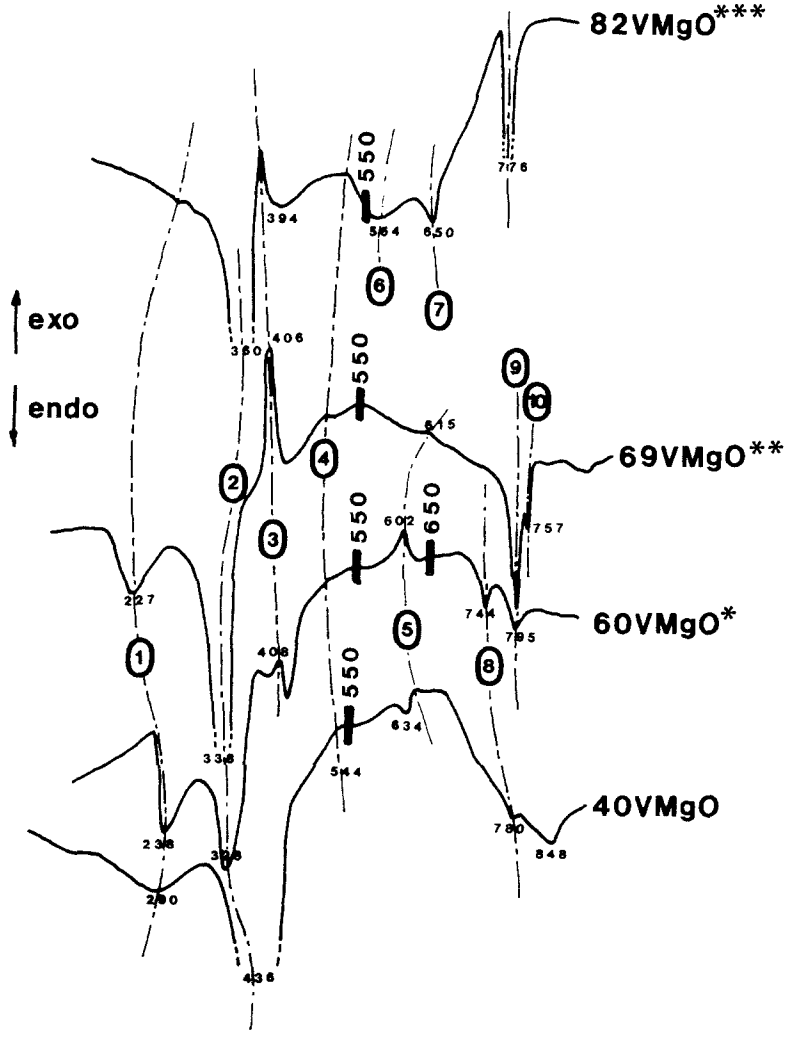

FIG. 2. DTA curves for VMgO catalysts. *Nominal content corresponding to $Mg_3V_2O_8$; **nominal content corresponding to $Mg_2V_2O_7$; ***nominal content corresponding to MgV_2O_6.

which are listed in Table 3. Events 1 and 2, which correspond to endothermic phenomena, are attributed respectively to the decomposition of NH_4VO_3 and $Mg(OH)_2$. It is interesting to note how the vanadium content changes the position of the peaks and their forms. For the 40 VMgO, the $Mg(OH)_2$ decomposition is highly delayed. The formation of $\alpha Mg_2V_2O_7$ is observed around 400°C (peak 3). The formation of $Mg_3V_2O_8$ is observed around 600°C (peak

TABLE 3

Transformations of the Oxides

(1) $2NH_4VO_3(s) \rightarrow V_2O_5(s) + 2NH_3(g) + H_2O(g)$
(2) $Mg(OH)_2(s) \rightarrow MgO(s) + H_2O(g)$
(3) $2MgO(s) + V_2O_5(s) \rightarrow \alpha Mg_2V_2O_7(s)$
(4) $3MgO(s) + V_2O_5(s) \rightarrow \alpha Mg_3V_2O_8(s)$
(5) $\alpha MgV_2O_6(s) \rightarrow \beta MgV_2O_6(s)$
(6) $V_2O_5(s) \rightarrow V_2O_5(l)$
(7) $2\beta MgV_2O_6(s) \rightarrow \alpha Mg_2V_2O_7(s) + V_2O_5(l)$
(8) $\alpha Mg_2V_2O_7(s) \rightarrow \beta Mg_2V_2O_7(s)$

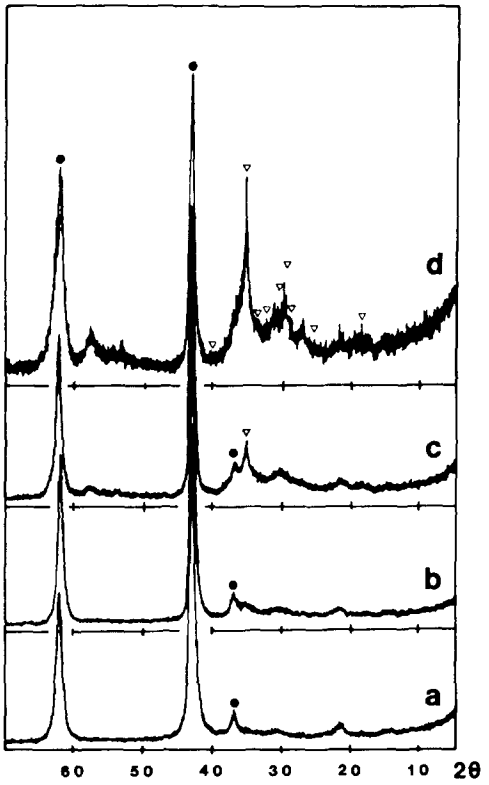

FIG. 3. X-ray diagrams of VMgO catalysts. (a) 5 VMgO, (b) 13 VMgO, (c) 29 VMgO, (d) 40 VMgO. (●) MgO, (▽) $\alpha Mg_2V_2O_7$.

4). Further events correspond to polymorphic transitions or melting of the different phases. From this study it can be explained why $\alpha Mg_2V_2O_7$ exists as traces in reference $Mg_3V_2O_8$ and βMgV_2O_6 as traces in reference $\alpha Mg_2V_2O_7$.

Results of X-ray diffraction for catalysts calcined at 550°C are presented in Figs. 3 and 4 from 5 to 69 nominal content of V_2O_5. At low vanadium content, diffraction lines of MgO only are observed. At 29 V_2O_5 nominal content, the $\alpha Mg_2V_2O_7$ phase superimposed on MgO can be observed. Both $Mg_3V_2O_8$ and $\alpha Mg_2V_2O_7$ are then observed for 40, 48, and 60 V–Mg–O. For 69 V–Mg–O, $\alpha Mg_2V_2O_7$ is dominant with traces of $Mg_3V_2O_8$ and αMgV_2O_6. 82 V–Mg–O, which for simplification is not presented here, was characteristic of βMgV_2O_6 with $\alpha Mg_2V_2O_7$ and traces of V_2O_5. This evolution is quite coherent with the DTA study (Fig. 2). Further evidence is observed for 60 V–Mg–O calcined at 550 and 650°C (Fig. 5): 650°C is higher than the temperature of formation of $Mg_3V_2O_8$. This point is very important because it can explain why the temperature of calcination of the catalysts is so important in promoting the effective phase responsible for the oxidative dehydrogenation. This will be discussed below.

The results of the electron microscopic investigation on the reference phases are shown in Fig. 6. The orthovanadate phase (Fig. 6a) appears to be constituted of large (1–2 μm) and small (20–30 nm) ovoid crystals. The STEM examination shows that

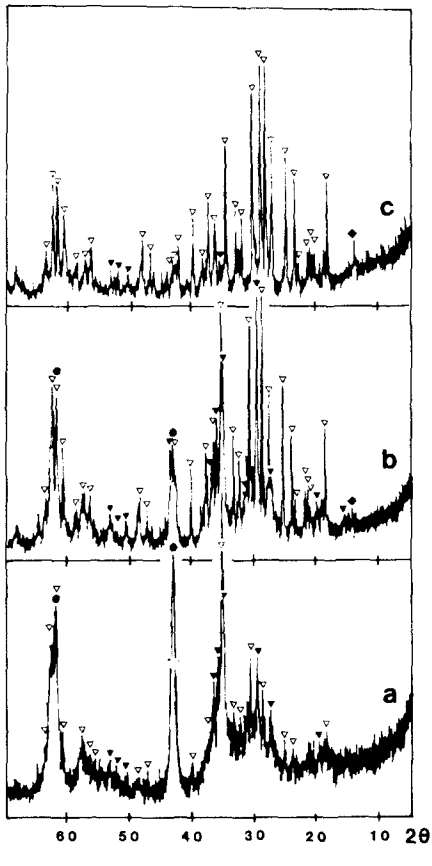

FIG. 4. X-ray diagrams of VMgO catalysts. (a) 48 VMgO, (b) 60 VMgO, (c) 69 VMgO. (●) MgO, (▼) $Mg_3V_2O_8$, (▽) $\alpha Mg_2V_2O_7$, (◆) αMgV_2O_6.

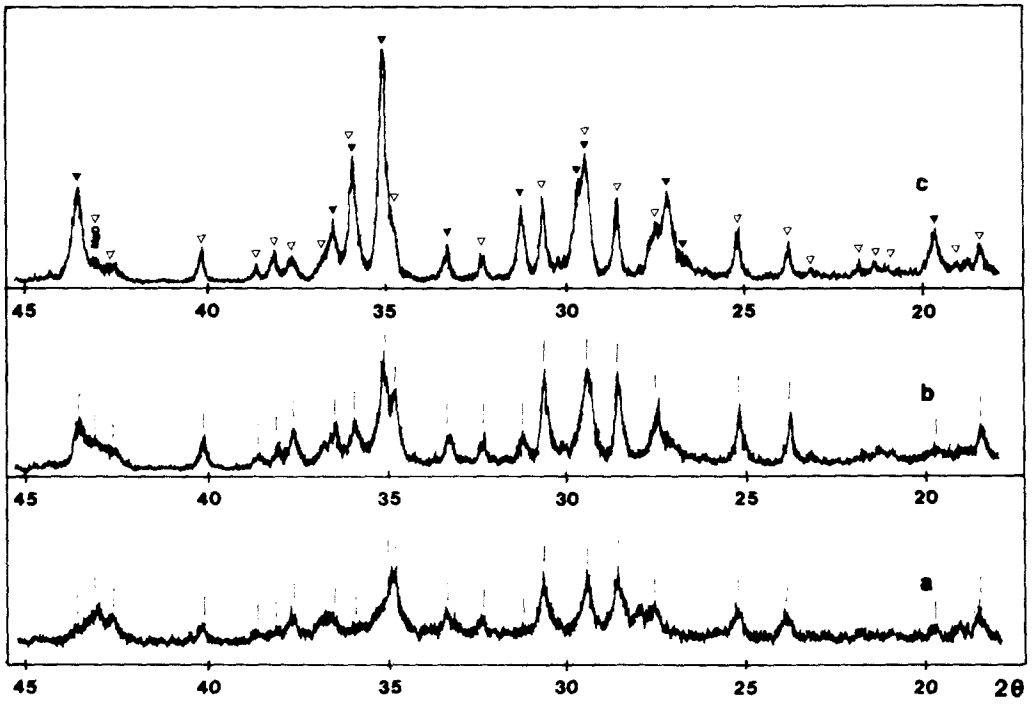

FIG. 5. Influence of calcination temperature on 60 VMgO ($\alpha Mg_2V_2O_7$). (a) 60 VMgO, 550°C; (b) 60 VMgO, 600°C; (c) 60 VMgO, 650°C. (▽) $\alpha Mg_2V_2O_7$, (▼) $Mg_3V_2O_8$.

the composition is homogeneous and all the ovoid crystals contain both V and Mg in the ratio Mg/(Mg + V) = 0.45. The difference from the theoretical ratio of 0.60 can be explained by the greater absorption of the Mg radiation by the detector window due to the low energy of the fluorescence emission of Mg$K\alpha$. The pyrovanadate phase (Fig. 6b) appears to consist of better-defined parallelepipeds (200 nm–1 μm) again with a homogeneous composition and a ratio Mg/(Mg + V = 0.35 (theor. 0.5). The metavanadate phase (Fig. 6c) presents platelets with various shapes (5 nm–1 μm) with a good homogeneity in the composition and a Mg/(Mg + V) ratio = 0.10 (theor. 0.33). The two catalysts 40 V–Mg–O and 60 V–Mg–O calcined at 550°C were examined by TEM and STEM (Figs. 7 and 7b). 40 V–Mg–O looks like MgO with small crystallites arranged like aggregates with a more uniform size (10–50 nm). The STEM examination shows V and Mg all over the sample but with different Mg/(Mg + V) ratios varying from 0.50 to 0.90. Taking into account the previous study on the reference samples, the presence of the three vanadates associated with MgO can be postulated and their repartition is not homogeneous. The 60 V–Mg–O presents a more heterogeneous aspect with regions looking like 40 V–Mg–O (small crystallites, 10–50 nm) and regions with larger crystals (50–100 nm) with the specific shape characteristic of $\alpha Mg_2V_2O_7$. The STEM examination confirms the two Mg/(Mg + V) ratios characteristic of the two families (0.5–0.9 for the first and 0.35 for the second). This corresponds to dispersion of vanadates on MgO in the small crystallites and larger $\alpha Mg_2V_2O_7$ crystals, which is in agreement with the X-ray diffraction study (Fig. 5a). Calcination of this catalyst at 650°C implies a sintering of the two families. The STEM examination shows that the Mg/(Mg + V) ratio of the smaller family is then more centered

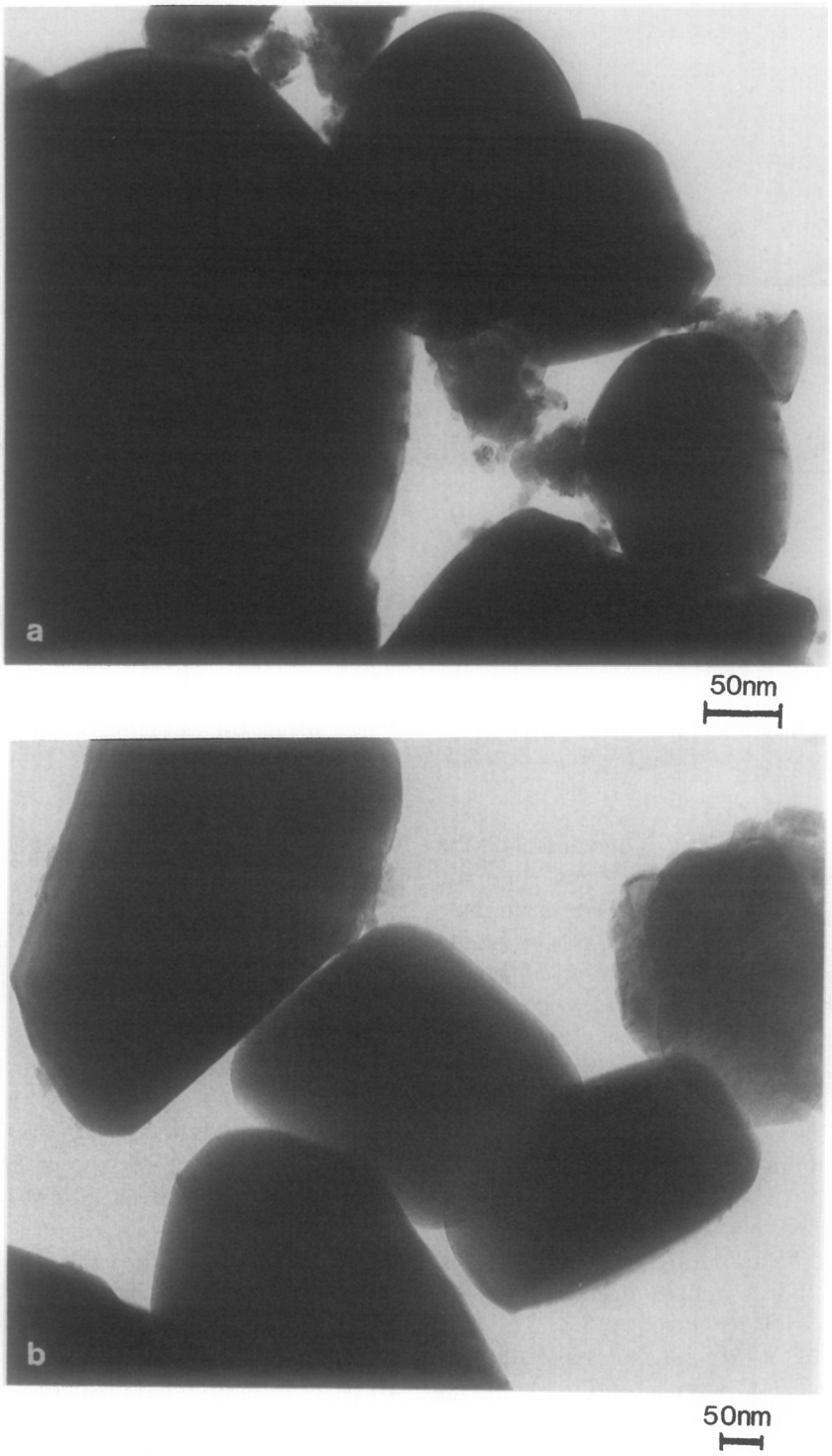

FIG. 6. TEM examination of the reference phases. (a) $\beta Mg_3V_2O_8$; (b) $\alpha Mg_2V_2O_7$; (c) βMgV_2O_6

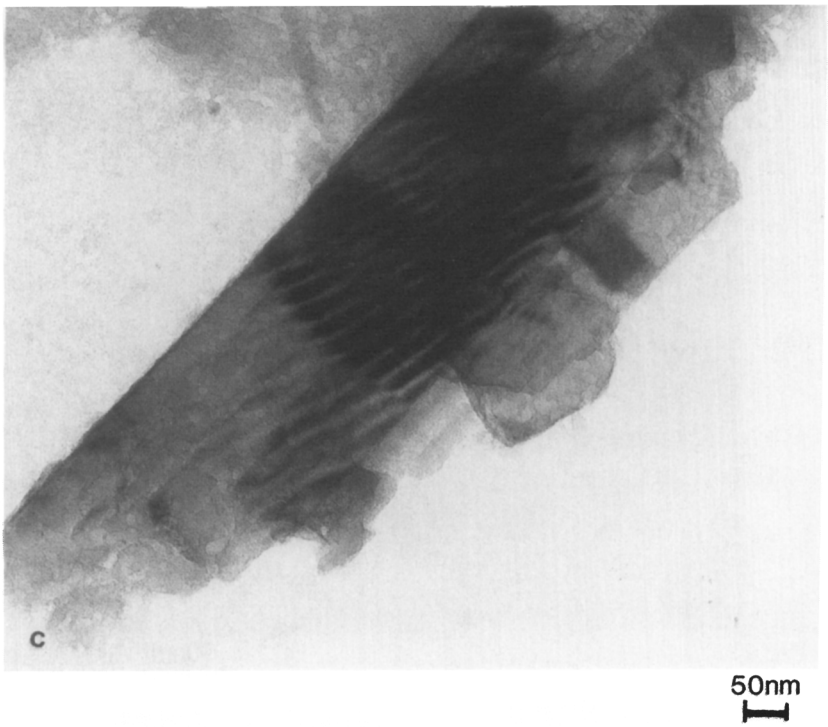

FIG. 6—*Continued*

around 0.5 while the larger family gives a Mg/(Mg + V) ratio characteristic of $Mg_3V_2O_8$(0.45) in agreement with the evolution of the X-ray diagram (Fig. 5c).

Infrared spectra of the reference phases are presented in Fig. 8. Our results are compared in Table 4 with those of Hanuza and co-workers (*9*) and Kung and co-workers (*1, 2*). There is a good agreement between the different results. However, we think that some of their peak assignments are questionable and we are of the opinion that they may be due to the presence of some impurities. Thus the ν_{AS}(VOV) at 715 cm^{-1} and the ν_S(VOV) at 535 cm^{-1}, observed by Hanuza and co-workers for $\alpha Mg_2V_2O_7$, should be attributed to the presence of small amounts of $Mg_3V_2O_8$ and αMgV_2O_6, respectively. This is also the case for the $\delta_S(VO_6)$ in αMgV_2O_6 at 406 cm^{-1}, which should be attributed to the presence of small amounts of $Mg_3V_2O_8$. It must be noted as previously mentioned by Kung and co-workers (*1, 2*), that the two bands at 975 and 965 cm^{-1} specific of the $V^V{=}O$ bond is characteristic of the pyrovanadate $\alpha Mg_2V_2O_7$. The poor resolution of the spectrum of αMgV_2O_6 in comparison with the other two spectra is indicative of a higher distortion of the local structure of the oxygens around the vanadium. The infrared spectra of the catalysts calcined at 550°C is given in Fig. 9. They confirm the X-ray diffraction study. The 60 V–Mg–O with the nominal composition of the orthovanadate is more typical of the pyrovanadate with its characteristic bands (360, 380, 440, 575, 668, 692, 821, 850, 965, 977 cm^{-1}). The presence of the orthovanadate is visible with a band at 337 cm^{-1} and a shoulder at 715 cm^{-1}. The spectrum of 69 V–Mg–O is identical to that of $\alpha Mg_2V_2O_7$.

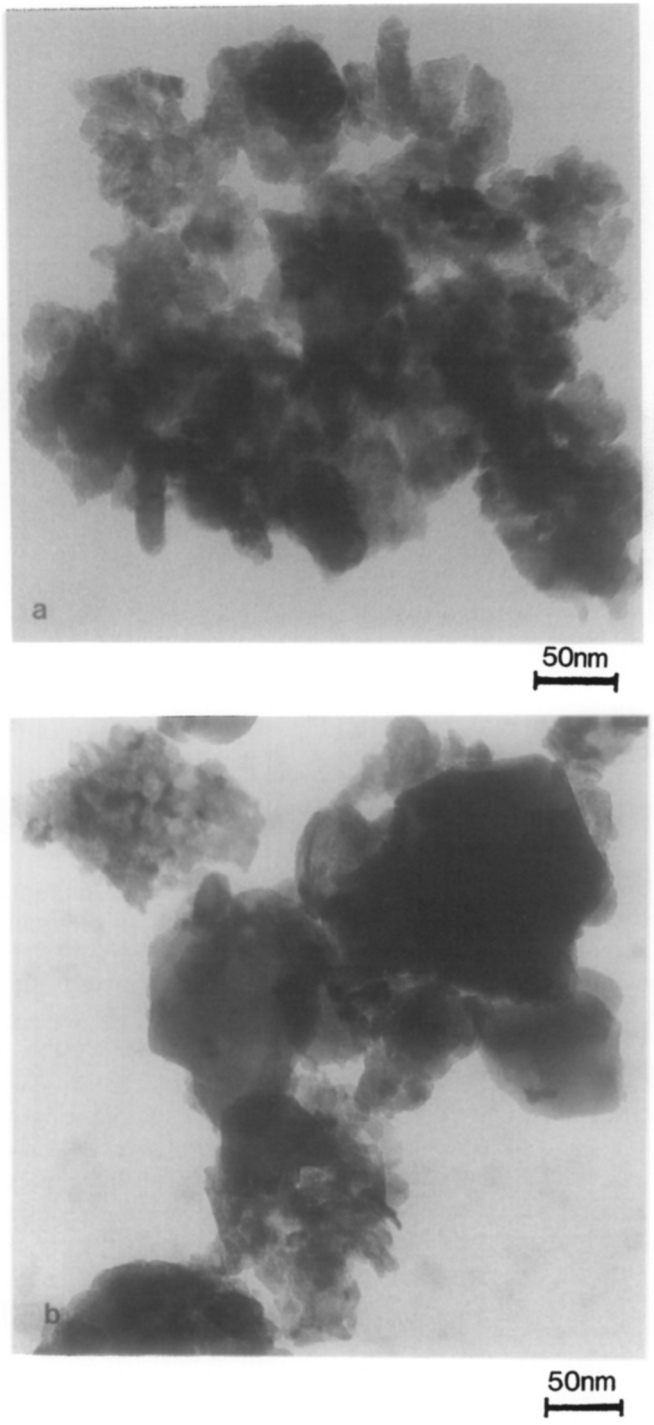

FIG. 7. TEM examination of the VMgO catalysts. (a) 40 VMgO, 550°C; (b) 60 VMgO, 550°C; (c) 60 VMgO, 650°C.

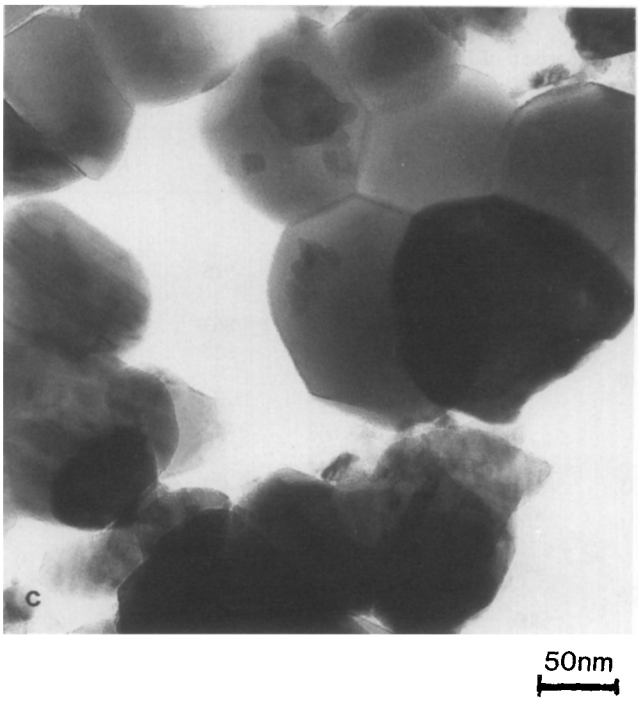

FIG. 7—*Continued*

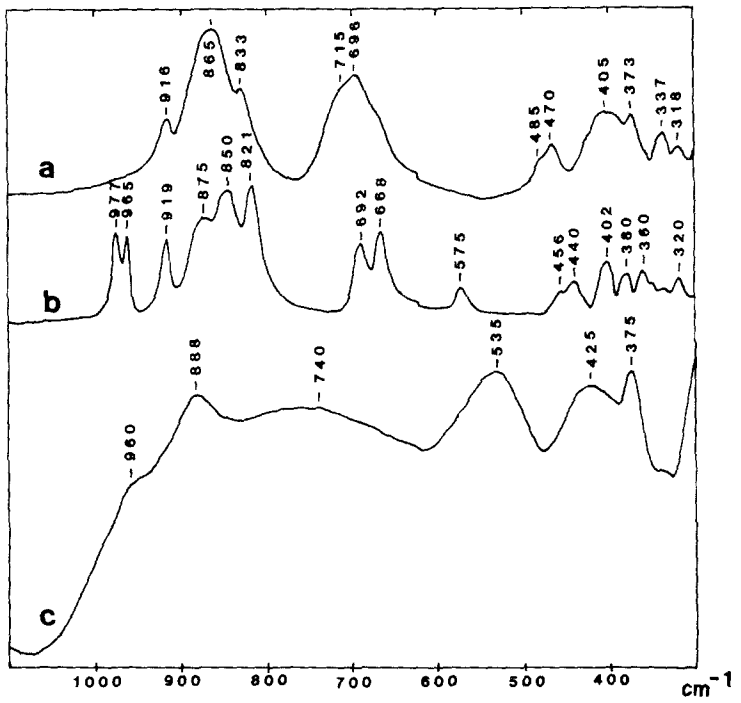

FIG. 8. Infrared spectra of the reference phases. (a) $Mg_3V_2O_8$, (b) $\alpha Mg_2V_2O_7$, (c) βMgV_2O_6.

TABLE 4

Comparison of IR Peak Assignments of the Reference Phases

αMgV_2O_6			$\alpha Mg_2V_2O_7$			$\alpha Mg_3V_2O_8$			Assignment[a]
H^a	K^b	or[c]	H^a	K^b	or[c]	H^a	K^b	or[c]	
950		960	986	972	977				$^{IV}V^{V} = O$ and $^{IV}_{S}(VO_4)$
					965				
			926		919	915		916	
883		888	873						$\nu_{AS}(VO_4)$ and $\nu_{AS}(VO_6)$
			856			863	859	865	
			815	820	821	827	834	833	
740		740	715					715	$\nu_{AS}(VOV)$
					692	695	700	696	
				666	668				
				574	575			485	$\nu_S(VOV)$
530	549	535	535			477		470	
			472			464	463		$\delta_S(VO_4)$ and $\delta_S(VO_6)$
					456				
			440	444	440				
428		425							
406			400	402	395		405		
			390						
373		375	381			369		373	$\delta_{AS}(VO_4)$ and $\delta_{AS}(VO_6)$
					360				
						341			
341			334			334		337	
					320	316		318	
300			305						

[a] According to Hanuza (*9*)

[b] According to Kung (*1*, *2*). Only quoted values indexed.

[c] Our results.

The surface compositions of the reference phases and of the catalyst were determined by XPS measurement. The atomic ratios are given by the approximate relationship: $n_1/n_2 = I_1/I_2 \times (\sigma_2 \sqrt{E_{k2}}/\sigma_1 \sqrt{E_{k1}})$, where σ is the cross section of ejected electrons calculated and tabulated by Scofield (*10*), E_{k1} and E_{k2} are the kinetic energies of the electrons, and I_1 and I_2 are the area of peaks corresponding to elements 1 and 2. Binding energy values for the $V_{2p_{3/2}}$ level were previously determined as being equal to 516.8 ± 0.2 eV for V_2O_5 and 515.7 ± 0.2 eV for V_2O_4 (*11*). The results are presented in Table 5. It appears that the binding energy values for $V_{2p_{3/2}}$ on all samples is higher than 516.8 eV corresponding to $V_2O_5(V^{5+})$ but the values are not in agreement with those published by Kung and co-workers (*2*). Indeed it appears that the samples with a low V content present a lower binding energy (517.0 eV) for $Mg_3V_2O_8$ and 40 VMgO. The binding energy values depend not only on the oxidation state but also on the covalent character of ion–ligand bonds.

TABLE 5

XPS Results

Samples	E_L $V_{2p3/2}$ (eV)	Mg_{2p}/O_{1s}	$V_{2p3/2}/O_{1s}$	$Mg_{2p}/V_{2p3/2}$
$Mg_3V_2O_8$	517.0	0.705	0.23	3.1
$\alpha Mg_2V_2O_7$	518.1	0.77	0.27	2.9
βMgV_2O_6	518.0	0.42	0.34	1.2
40VMgO 550	517.0	1.0	0.10	10.0
60VMgO 550	518.2	0.44	0.21	2.1

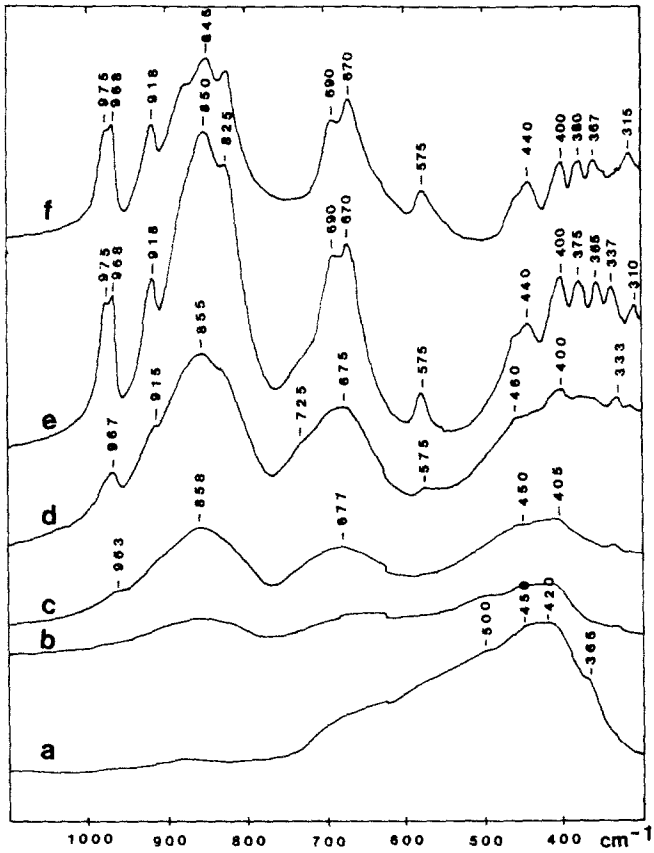

FIG. 9. Infrared spectra of the VMgO catalysts (calcined at 550°C). (a) MgO, (b) 29 VMgO, (c) 40 VMgO, (d) 48 VMgO, (e) 60 VMgO, (f) 69 VMgO.

The Mg/V ratios for the reference phases were observed to be higher than the expected theorical value. Thus, it can be concluded that a superficial enrichment in Mg occurs on the crystal of the three magnesium vanadates.

Before discussing the results of the ^{51}V NMR studies, it appears important to present some information on the structure of the three magnesium vanadates and the local environment of the vanadium atoms with respect to the O and Mg atoms.

Magnesium orthovanadate $Mg_3V_2O_8$ crystallizes in the orthorhombic space group C_{mca} with $a = 0.605$, $b = 1.144$, and $c = 0.833$ nm and $Z = 4$. The structure was refined by Krishnamachari and Calvo (*12*). It consists of nearly cubic closest packing of oxygen atom layers with the Mg ions in octahedral sites and the V ions in tetrahedral sites (Fig. 10). The VO_4 tetrahedron is presented in Fig. 11a. The O packing

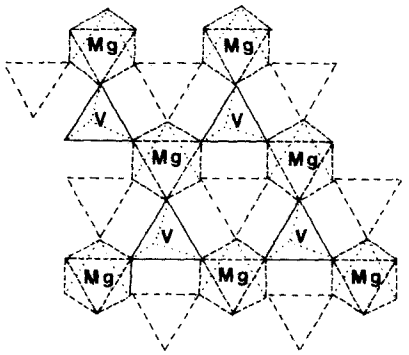

FIG. 10. Structure of $Mg_3V_2O_8$ (from Ref. (*12*)).

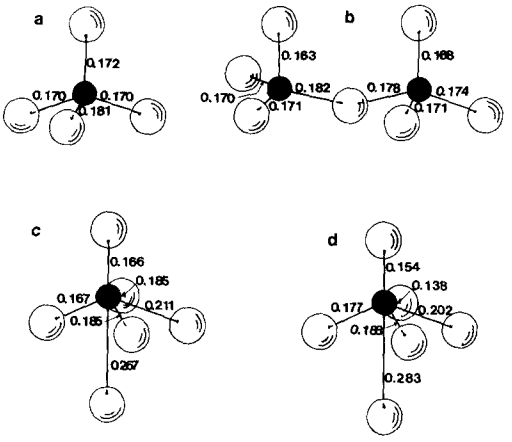

FIG. 11. Local environment of vanadium (distances are given in nanometers). (a) $Mg_3V_2O_8$, (b) $Mg_2V_2O_7$, (c) MgV_2O_6, (d) V_2O_5. As the local structure of $\alpha Mg_2V_2O_7$ is not yet known and as $\alpha Mg_2V_2O_7$ is quite similar to β, Fig. 11b gives the local structure of $\beta Mg_2V_2O_7$ (*13*).

around the V atom is highly constricted, corresponding to a more covalent character in agreement with the XPS observations. Magnesium pyrovanadate, $\alpha Mg_2V_2O_7$, crystallizes in the monoclinic space group $P_{2_1/c}$ with $a = 0.660$, $b = 0.841$, $c = 0.949$ nm and $\beta = 100.61°$. The structure given by Clark and Morley (*6*) consists of rows of V_2O_7 groups with long V–O bridges within these groups (Fig. 12). Each of the terminal oxygen atoms of the V_2O_7 groups are shared with two Mg ions, except O of the shortest 0.163 nm bond which is connected to only one Mg ion (*13*) (Fig. 11b). Due to the distortion of the V_1O_4 tetrahedron and to a minor degree of the $V_{11}O_4$ tetrahedron, the V–O bonds are less covalent in agreement with the XPS observations. Magnesium metavanadate, αMgV_2O_6, crystallizes in the monoclinic space group $C_{2/m}$ with $a = 0.928$, $b = 0.350$, $c = 0.673$ nm and $\beta = 111.77°$ with $Z = 2$. The structure was refined by Ng (*14*). It consists of VO_6 octahedra joined by edges and connected together through MgO_6 octahedra (Fig. 13). The VO_6 octahedron appears highly distorted (Fig. 11c) as in V_2O_5 (Fig. 11d). The ionic character of the V–O bonds appears important in agreement with the XPS observations.

From this presentation it appears that there are different coordinations of vanadium species (*9*). ^{51}V NMR provides valuable information about the structure of the local vanadium environment (*15*). This should lead to various ^{51}V NMR spectra for the different vanadates. The spectra, illustrated in Figs. 14, 15, and 16, are comparable with those of Lapina *et al.* (*15*): the $Mg_3V_2O_8$ presents a very narrow signal ($\delta = -550$ ppm), showing the absence of quadrupolar interaction. With no spinning, the

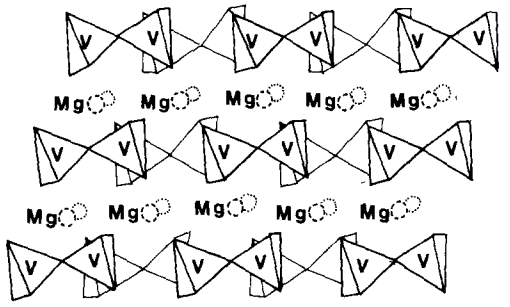

FIG. 12. Structure of $\alpha Mg_2V_2O_7$ (from Ref. (*13*)). MgO_6 octahedra between the V_2O_7 groups are only positioned with the Mg center atom.

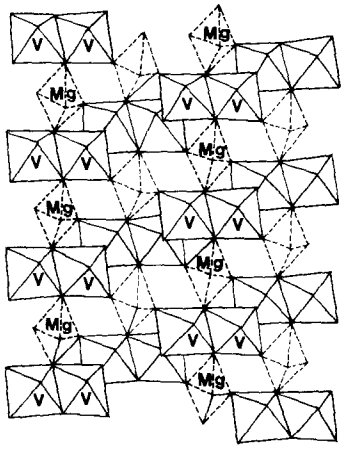

FIG. 13. Structure of βMgV_2O_6 from Ref. (*14*)). Only the O atoms on the top of the VO_6 octahedra joined by edges have been represented.

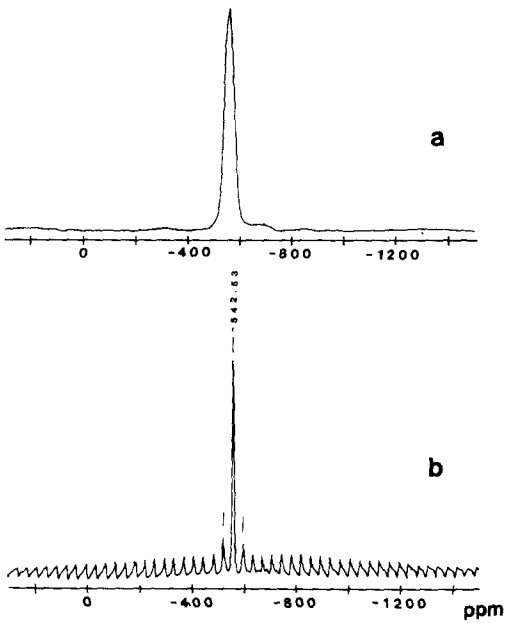

FIG. 14. ^{51}V NMR spectra of $Mg_3V_2O_8$ (a) without spinning, (b) with spinning.

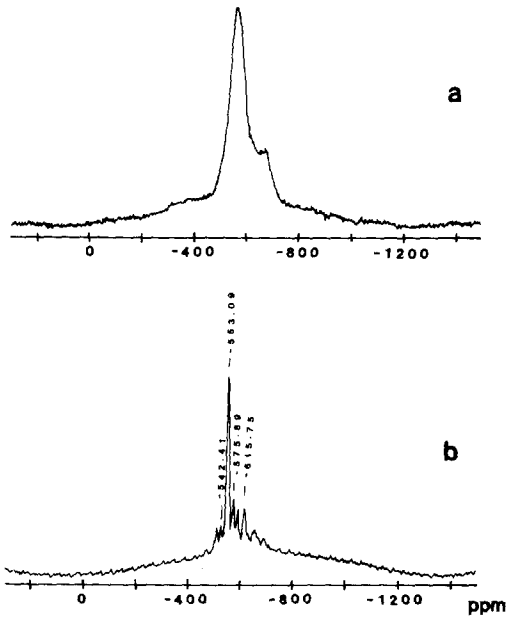

FIG. 15. ^{51}V NMR spectra of $\alpha Mg_2V_2O_7$ (a) without spinning, (b) with spinning.

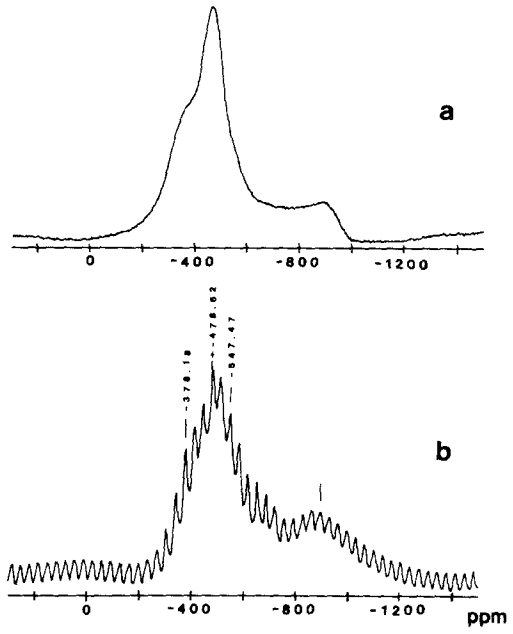

FIG. 16. ^{51}V NMR spectra of βMgV_2O_6 (a) without spinning, (b) with spinning.

signal is still narrow, showing a low chemical shift anisotropy. This result is quite in agreement with the high symmetry of the vanadium environment (Fig. 11a). The spectrum of $\alpha Mg_2V_2O_7$ presents two signals ($\delta_1 = -615$ ppm and $\delta_2 = -550$ ppm) with a higher density for the second one. The narrow width of these peaks is, as previously, indicative of a low quadrupolar interaction. The presence of two signals is in agreement with the local vanadium structure of the V_2O_7 groups showing two V sites in 1/1 ratio. The NMR spectrum of the sample without spinning shows the presence of a chemical shift anisotropy for at least one peak. This is in agreement with the fact that for V_{II} there is an environment of vanadium which is very similar to that of $Mg_3V_2O_8$ and thus relatively symmetrical, while for V_I the VO_4 distortion is higher, which corresponds to a higher chemical shift anisotropy. Consequently we can propose the attribution of the peak at -620 ppm to V_I and of the peak at -550 ppm to V_{II}, the lower

TABLE 6

Catalytic Result for Propane Oxidation at 550°C on the Reference Phases

Samples	BET area (m^2/g)	Conversion C_3H_8 (%)	Selectivity(%)				
			C_3H_6	CO_2	CO	Oxygenates detected	
$Mg_3V_2O_8$ 1.0g	0.9	8.3	6.0	94.0	—	—	
$\alpha Mg_2V_2O_7$ 0.2g	1.7	6.9	53.5	18.8	10.4	Acrylald.	12.0
						Propanal	3.5
						Acetic Acid	1.0
αMgV_2O_6 0.7g	0.1	7.4	14.9	17.6	36.6	Ethanal	30.2

intensity of the former signal coming from the transfer of the signal toward the rotation bands. The spectrum of MgV_2O_6 (Fig. 16) is different with a very high quadrupolar interaction (*15*). The observed value (~800 ppm), which is similar to that which is observed for V_2O_5 (*17*), corresponds to the high distortion of the VO_6 octahedron.

Reaction Study

Catalytic oxydehydrogenation of propane was studied on the reference phases. The results are summarized in Table 6 for the catalytic test performed at 550°C. It clearly appears that the pyrovanadate, $\alpha Mg_2V_2O_7$, is both more active and more selective for the oxydehydrogenation of propane to propene, with the formation of a small extent of oxygenates, principally acrylaldehyde. On the contrary, the orthovanadate, $Mg_3V_2O_8$, is responsible for total oxidation. Metavanadate, αMgV_2O_6, is not very selective for oxydehydrogenation and leads to a high extent of ethanal. Fig. 17 presents the catalytic result at 500°C as a function of the vanadium content (expressed as the weight percentage of V_2O_5) for V–Mg–O catalysts calcined at 550°C. Propane conversion gives two maxima for 13 and 69 VMgO while the selectivity to propene increases steadily and is maximal for the 69 VMgO catalyst. Figure 18 presents the catalytic results at 550°C for the same catalysts. The general trend of the evolution is the same. From these results, it can be observed that maximum yields to propene are obtained for the intermediate vanadium content (40–69) for which all the physicochemical characterizations ascertain the presence, in common, of $\alpha Mg_2V_2O_7$. This point will be discussed below. Figure 19 brings another proof of the unique role of the pyrovanadate phase. Indeed the same curve of propene selectivity versus propane conversion can be drawn both for 40 and 60 VMgO 550. These catalysts were examined after the reaction. No change was observed either by IR or by XRD examination.

The negative role of the orthovanadate

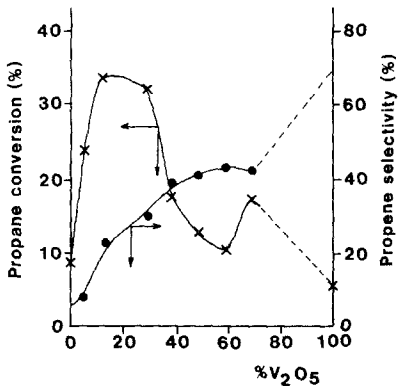

FIG. 17. Catalytic results for propane oxidation on the VMgO catalysts at 500°C. Catalytic conditions: m = 0.3 g, propane/air = 2/98, and flow rate = 50 ml · min^{-1}.

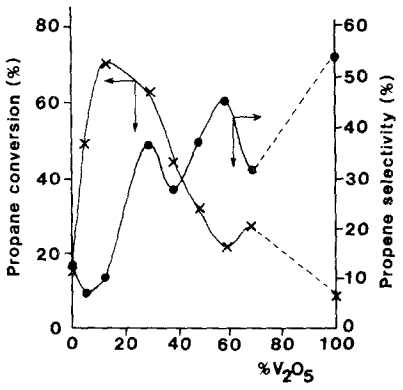

FIG. 18. Catalytic results for propane oxidation on the VMgO catalysts at 550°C. Catalytic conditions: m = 0.3 g, propane/air = 2/98, and flow rate = 50 ml · min^{-1}.

appears also in Fig. 20. It was previously shown by X-ray diffraction, infrared spectroscopy and STEM that the calcination of 60 VMgO from 550 to 650°C involved a modification of the catalyst from a solid which was more typical of $\alpha Mg_2V_2O_7$ to $Mg_3V_2O_8$. This is associated with a decrease in the propene yield (Fig. 20). The higher stability of propene in contact with $\alpha Mg_2V_2O_7$ can be compared to that of the other phases in the course of propene oxidation at 550°C with low propene/oxygen ratio. (In order to get a better sensitivity on the detection of the oxygenates, a propene/

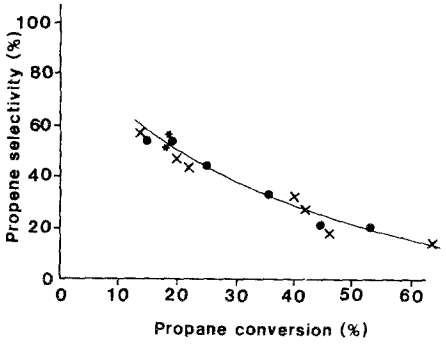

FIG. 19. Propene selectivity versus propane conversion. (×) 40 VMgO, 550°C, (●) 60 VMgO, 550°C, (*) $\alpha Mg_2V_2O_7$ (reference phase).

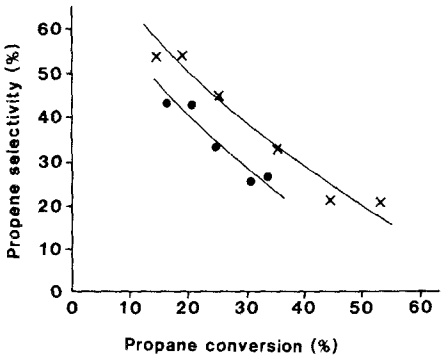

FIG. 20. Propene selectivity versus propane conversion. (×) 60 VMgO, 550°C, (●) 60 VMgO, 650°C.

air ratio of 2% was chosen, which approximates the conditions of propane oxidation for a total of transformation of propane to propene.) The results are presented in Table 7. Propene is totally oxidized, principally to CO_2, on $Mg_3V_2O_8$ whereas on βMgV_2O_6 we observe principally the formation of CO and ethanal. On the contrary, $\alpha Mg_2V_2O_7$ gives lower amounts of CO and CO_2 but higher amounts of oxygenates, principally acrylaldehyde. These results confirm the classification of the three magnesium vanadates for propane oxidation and confirm the possibility of a direct route from propane to propene and oxygenates on $\alpha Mg_2V_2O_7$.

DISCUSSION

Our data show that magnesium pyrovanadate is the active phase for oxidative dehydrogenation of propane to propene. This has been established by characterization of the three magnesium vanadates by X-ray diffraction, infrared spectroscopy, TEM and STEM, XPS and ^{51}V NMR, and subsequent study of their catalytic properties for this reaction. The specificity of $\alpha Mg_2V_2O_7$ was further confirmed by propene oxidation. Our conclusion is at variance with the proposals of Kung *et al.* (*2*, *3*) who propose that magnesium orthovanadate $Mg_3V_2O_8$ is the active phase. Furthermore, in this latter phase,

TABLE 7

Catalytic Results for Propene Oxidation on the Reference Phases at 550°C

Samples	Conversion (%)		Selectivity (%)			
	C_3H_6	O_2	CO_2	CO	C_2H_4	Oxygenates
$Mg_3V_2O_8$ 0.075g $S = 0.9$ m²/g	35.8	22.1	88.8	15.9	0	0
$\alpha Mg_2V_2O_7$ 0.3g $S = 1.7$ m²/g	38.3	13.5	15.8	32.6	0.15	Acrylaldehyde 35.0 Propanal 11.1 Acetic acid 3.0
αMgV_2O_6 0.6g $S = 0.1$ m²/g	37.8	15.2	28.2	38.6	0.98	Ethanal 30.0
Empty reactor	2.9	0.2	+	+	+	0

vanadium occupies isolated tetrahedral sites which are unfavorable for selective oxidation. This conclusion is confirmed by the calcination of 60 VMgO from 550 to 650°C, which develops $Mg_3V_2O_8$ and consequently decreases the oxydehydrogenation to propene.

In order to define the nature of the oxygen responsible for the oxydehydrogenation, we performed a catalytic test without oxygen in the flow (oxygen was replaced by nitrogen). Propene is observed from the very beginning but the conversion and the selectivity to propene diminish with time but not abruptly. After regeneration under air at 500°C for 3 h and purging under nitrogen, the catalytic performances are restored with a lower conversion. Consequently, the oxidative dehydrogenation of propane needs nonmolecular oxygen, which suggests a Mars and Van Krevelen type of mechanism, but little more can be said about the nature of this oxygen, in particular whether it is bulk or chemisorbed oxygen.

The unique feature of $\alpha Mg_2V_2O_7$ is the presence of the $V_I{=}O$ short bond which could initiate a H abstraction. The bridging O of the $V_I{-}O{-}V_{II}$ bond could participate in the oxydehydrogenation mechanism for the formation of water. All these steps could take place simultaneously giving rise to a dynamic model in which the local structure should change from the $V_2O_7^{4-}$ unit to two square-based $MgVO_3$ units (*18*).

ACKNOWLEDGMENTS

The authors are indebted to Mrs. C. Leclercq for the electronic microscopy study of the catalysts and to Dr. F. Lefebvre for the ^{51}V MAS NMR. They thank also Drs. J. C. Vedrine and R. P. A. Sneeden for fruitful discussion. The authors thank the ORKEM Co. for financial support.

REFERENCES

1. Chaar, M. A., Patel, D., Kung, M. C., and Kung, H. H., *J. Catal.* **105,** 483 (1987).
2. Patel, D., Kung, M. C., and Kung, H. H., *in* "Proceedings, 9th International Congress on Catalysis, Calgary, 1988" (M. J. Phillips and M. Ternan, Eds.), p. 1554. Chem. Institute of Canada, 1988.
3. Chaar, M. A., Patel, D., and Kung, H. H., *J. Catal.* **109,** 463 (1988).
4. Lubin and Ritterhaus, private communication, ASTM file No. 19-779, 1966.
5. Wollast, R., and Tazairt, A., *Silic. Ind.* **34,** 37 (1969).
6. Clark, G. M., and Morley, R., *J. Solid State Chem.* **16,** 429 (1976).
7. Galy and Pouchard, *Bull. Soc. Chim. Fr.* **261** (1967) [ASTM file No. 23-1233].
8. Parker, F., and Cauley, Mc., private communication, ASTM file No. 34-13.
9. Hanuza, J., Jerowska-Trzebiatowska, B., and Oganowski, W., *J. Mol. Catal.* **29,** 109 (1985).

10. Scofield, J. M., *J. Electron Spectrosc. Relat. Phenom.* **8,** 129 (1976).
11. Blaauw, C., Leenhouts, F., Van der woode F., and Sawatzky, G. A., *J. Phys. C.* **8,** 459 (1976).
12. Krishnamachari, N., and Calvo, C., *Canad. J. Chem.* **49,** 1630 (1971).
13. Gopal, R., and Calvo, C., *Acta Crystallogr. Sect. B* **30,** 2491 (1974).
14. Ng, H. N., and Calvo, C., *Canad. J. Chem.* **50,** 3619 (1972).
15. Lapina, O. B., Simakov, A. V., Mastikhin, V. M., Veniaminov, S. A., and Shubin, A. A., *J. Mol. Catal.* **50,** 55 (1989).
16. Chary, K. V. R., Venkat Rao, V., and Mastikhin, V. M., *J. Chem. Soc. Chem. Comm.*, 202 (1989).
17. Vedrine, J. C., Millet, J. M., and Volta, J. C., *Faraday Discuss. Chem. Soc.* **87,** 230 (1989).
18. Bouloux, J. C., Milosevic, I., and Galy, J., *J. Solid State Chem.* **16,** 393 (1976).